A hybrid reconstruction method for quantitative PAT

Kui Ren* Hao Gao† Hongkai Zhao‡

January 20, 2012

Abstract

The objective of quantitative photoacoustic tomography (qPAT) is to reconstruct the diffusion and absorption properties of a medium from data of absorbed energy distribution inside the medium. Mathematically, qPAT can be formulated as an inverse coefficient problem for the diffusion equation. Past research showed that if the boundary values of the coefficients are known, then the interior values of the coefficients can be uniquely and stably reconstructed with two well-chosen data sets. We propose a hybrid numerical reconstruction procedure for qPAT that uses both interior energy data and boundary current data, which is usually available in diffuse optical tomography. We show that these data allow the unique reconstruction of the boundary and interior values of the coefficients. The numerical implementation is based on reformulating the inverse coefficient problem as a nonlinear optimization problem. An explicit reconstruction scheme is utilized to eliminate the unknown coefficients inside the medium so that we only need to minimize over the boundary values, which significantly fewer degrees of freedom. Numerical simulations with synthetic data are presented to validate the method.

Key words. Quantitative photoacoustic tomography, diffuse optical tomography, inverse problem, diffusion equation, interior data, boundary data, hybrid reconstruction algorithm, numerical minimization, vector field method.

1 Introduction

Photoacoustic tomography (PAT) is a new hybrid biomedical imaging modality that attempts to combine classical ultrasound imaging techniques with diffuse optical tomography (DOT) techniques to achieve both high contrast and high resolution in imaging. In PAT, near infra-red (NIR) light are sent into a biological tissue. The tissue absorbs part of the incoming light and heats up due to the absorbed energy. The heating then results in expansions of the tissue and the expansion generates compressive (acoustic) waves. The time-dependent acoustic signal arrived on the surface of the tissue are then measured with

*Department of Mathematics, University of Texas at Austin, Austin, TX 78712; ren@math.utexas.edu .
†Department of Mathematics, University of California, Los Angeles, CA 90095; haog@math.ucla.edu .
‡Department of Mathematics, University of California, Irvine, CA 92697; zhao@math.uci.edu .

acoustic devices. From the knowledge of these acoustic measurements, one is interested in reconstructing the diffusion, absorption and thermal expansion properties of the tissue; see [2, 6, 16, 30, 32, 35, 41, 45, 49, 50, 51] for overviews of PAT.

Image reconstruction in PAT is a two-step process. In the first step, one uses the boundary acoustic signal to reconstruct the absorbed energy distribution inside the tissue. This step has been extensively studied in the past decade. When the acoustic wave speed is assumed to be constant, there are analytical reconstruction formulas in many settings [1, 13, 18, 19, 24, 23, 31, 33, 39, 41, 48, 47]. When the wave speed varies inside the medium, the reconstruction becomes more complicated; see [25, 26, 46, 42] for the analysis and simulation of this inverse problem. We assume in this paper that the first step has been done and thus we are given the data of the absorbed energy map in the domain, up to the boundary. We are thus interested in the second step of PAT, called quantitative PAT (qPAT), where we aim at reconstructing the absorption and diffusion properties of the tissue from this given data [3, 4, 7, 8, 10, 11, 14, 15, 17, 21, 20, 34, 44, 52, 53].

The propagation of NIR photons in biological tissues is often modeled by the diffusion equation. Let us denote by $X \subset \mathbb{R}^d$ $(d = 2, 3)$ the tissue of interest, with smooth boundary ∂X, and $u(\mathbf{x})$ the density of photons at position $\mathbf{x}$. Then $u(\mathbf{x})$ solves the following elliptic boundary value problem:

$$\begin{aligned} -\nabla \cdot D\nabla u + \sigma u &= 0, \quad \text{in } X \\ u + \gamma \mathbf{n} \cdot D\nabla u &= g, \quad \text{on } \partial X \end{aligned} \tag{1}$$

where $D(\mathbf{x}) > 0$ and $\sigma(\mathbf{x}) > 0$ are the diffusion and absorption coefficients of the tissue respectively, $\gamma > 0$ is the rescaled extrapolation length and g is the illumination source on the boundary. The outer unit normal vector of the domain boundary ∂X at $\mathbf{x}$ is denoted by $\mathbf{n}(\mathbf{x})$.

The initial pressure field, $H(\mathbf{x})$, that is generated due to the absorbed photon energy locally at location $\mathbf{x} \in \bar{X} \equiv X \cup \partial X$ is given as

$$H(\mathbf{x}) = \sigma(\mathbf{x})u(\mathbf{x}), \qquad \mathbf{x} \in \bar{X}. \tag{2}$$

Here we have assumed that all absorbed energy are converted into the pressure field, i.e., the photoacoustic efficiency, usually called the Grüneisen coefficient, is the constant one. This assumption is not necessary but only here to simplify the presentation in the follow sections. The reconstruction method we propose in this work can be extended straightforwardly to the case when the Grüneisen coefficient is a function of space and unknown, following the results in [8, 9, 10].

The objective of qPAT is to reconstruct the coefficients D and σ from the interior data H. This inverse problem is identical to the problem of diffuse optical tomography except that the photon current data used in DOT are only available on the boundary of the domain while in qPAT the absorbed energy data are available in the interior of the domain. It is shown in [8, 10], based on a slightly modified model, see (3) below, that due to use of interior data, the stability of the problem has been significantly improved compared to the optical tomography problem. In fact, it is shown that with only two data sets, H_1 constructed from illumination g_1 and H_2 constructed from illumination g_2, one can uniquely and stably reconstruct the two coefficients σ and D, provided that g_1 and g_2 are selected carefully and

the boundary values $D_{|\partial X}$ and $\sigma_{|\partial X}$ are known. Lipschitz type of stability estimates can be derived for the inverse problem [8, 10].

In [8], an explicit reconstruction method has been developed for qPAT, based on the simplified model (3). The method is called the vector field method which consists of two main steps. In the first step, one solves a transport equation with the velocity field constructed from the two data sets H_1 and H_2. In the second step, one solves an elliptic equation to obtain another functional of the two coefficients. It then remains to obtain the two coefficients from the two functionals that have been recovered. The advantage of the method is that it decomposes the nonlinear inverse problem essentially into two linear problems that we know how to solve efficiently and then a coupling procedure that is algebraic. The method is fast since it is non-iterative even though the inverse problem itself is nonlinear. The drawbacks of the original vector field method lie in the facts that the method only works when the diffusion coefficient is known on the boundary of the domain *a priori*, and that only the diffusion problem with Dirichlet boundary conditions can be handled.

In this work, we are interested in solving the inverse problem to the diffusion model (1) with data (2). We assume that the boundary value of the diffusion coefficient, $D_{|\partial X}$, is unknown and propose to use additional boundary photon current data, data usually measured in diffuse optical tomography, to reconstruct this boundary value. The additional boundary current measurements would also allow us to handle Robin type of boundary conditions. We combine the vector field method with an optimization based method to solve the whole problem with both interior and boundary data. The vector field method is used to eliminate the unknowns inside the domain so that the unknown to be reconstructed only lives on the boundary. This reduces the space of the optimization variable to a great extent. The method can be viewed as a kind of reduced space minimization method with efficient ways to perform the reduction. Also by using the optimization formulation one can naturally incorporate appropriate regularization term that may be necessary to deal with ill-posedness, measurement inconsistency and noise for this inverse problem.

The rest of the paper is structured as follows. In Section 2 we review briefly an explicit reconstruction method, the vector field method, for qPAT in diffusive regime. We also formulate the new inverse problem with hybrid data and generalize the vector field method to this new problem. In Section 3 we present in detail the hybrid reconstruction method for the full nonlinear inverse problem. We then present a linearized version of the method in Section 4. We present some numerical reconstructions with synthetic data in Section 5 to validate the hybrid method we proposed. Concluding remarks are offered in Section 6.

2 A hybrid reconstruction method

The first uniqueness and stability results regarding the inverse diffusion problem in qPAT was obtained in [8, 10]. The theory was based on the diffusion model with Dirichlet boundary condition:

$$-\nabla \cdot D\nabla u + \sigma u = 0, \quad \text{in } X, \qquad u = g(\mathbf{x}), \quad \text{on } \partial X. \tag{3}$$

The proof of the uniqueness and stability is constructive in the sense that it provides an explicit reconstruction method for the inverse problem. We now recall briefly this vector

field method. To do that, we denote by $W^{k,p}(X)$ the space of functions whose derivatives of order less than k are in $L^p(X)$, with $W^{1,2}(X) \equiv \mathcal{H}^1(X)$. We assume that:

(**A**) The domain X is simply-connected with smooth boundary ∂X. The optical coefficients $(D, \sigma) \in W^{1,\infty}(\bar{X}) \times W^{1,\infty}(\bar{X})$ and $0 < c_0 \leq D, \sigma \leq C_0 < \infty$ for some positive c_0 and C_0. The illumination $g(\mathbf{x})$ is the restriction of a $C^3(\bar{X})$ function on ∂X and $g(\mathbf{x})$ is positive, $g \geq \tilde{c}_0 > 0$ for some $\tilde{c}_0$.

With these assumptions, it follows from standard elliptic theory [22, 37] that both the equation (1) and the equation (3) admit a unique solution, positive a.e., of class $W^{3,q}(X)$, $1 \leq q < \infty$.

2.1 The vector field method

Let H_1 and H_2 be two sets of measured data set corresponding to the diffusion problem (3) with the illumination sources g_1 and g_2 respectively. Then some straightforward algebraic calculations, subtracting the result of multiplying u_2 to the equation for u_1 from the result of multiplying u_1 to the equation for u_2, show that

$$-\nabla \cdot (Du_1^2)\nabla \frac{u_2}{u_1} = 0, \quad \text{in} \quad X, \qquad \frac{u_2}{u_1}(\mathbf{x}) = \frac{g_2}{g_1}(\mathbf{x}), \quad \text{on} \quad \partial X. \tag{4}$$

This means that $\frac{u_2}{u_1}$ solves a diffusion equation with the diffusion coefficient $v_1^2 \equiv Du_1^2 = \frac{D}{\sigma^2}H_1^2$. Using the fact that $\frac{u_2}{u_1} = \frac{H_2}{H_1}$, we can rewrite (4) slightly to obtain

$$-\nabla \cdot \frac{D}{\sigma^2}H_1^2\nabla \frac{H_2}{H_1} = 0, \quad \text{in} \quad X, \qquad \frac{D}{\sigma^2}(\mathbf{x}) = D_{|\partial X}\frac{g_1^2}{H_{1|\partial X}^2}, \quad \text{on} \quad \partial X. \tag{5}$$

This equation is a transport equation for the unknown variable D/σ^2, with the *known* vector field $\beta \equiv H_1^2\nabla\frac{H_2}{H_1}$. If the boundary value of this variable is known, mainly $D_{|\partial X}$ is known, we can then solve this equation to reconstruct D/σ^2. The results developed in [8, 10] ensure that there exist g_1 and g_2 such that:

(**B**) The vector field β is of class $W^{1,\infty}(X)$ and does not vanish inside the domain, i.e., $|\beta| \geq \beta_0 > 0$ for some positive β_0.

This ensures that the transport equation (5) can be uniquely solved. Note that to solve the transport equation, we only need to know the boundary value on the part of the boundary where the vector field starts, i.e. where $\mathbf{n} \cdot \beta < 0$. Let us denote by this part of the boundary by Γ and define $\mu^2(\mathbf{x}) \equiv \frac{D}{\sigma^2}$, then the transport equation (5) can be re-written as

$$\nabla \cdot \mu^2\beta = 0, \quad \text{in} \quad X, \qquad \mu^2 = D_{|\Gamma}\frac{g_{1|\Gamma}^2}{H_{1|\Gamma}^2} \equiv \mu_{|\Gamma}^2, \quad \text{on} \quad \Gamma \subset \partial X. \tag{6}$$

Of course, the term $\dfrac{g_{1|\Gamma}^2}{H_{1|\Gamma}^2}$, i.e. boundary value of σ^2 can be replaced with $\dfrac{g_{2|\Gamma}^2}{H_{2|\Gamma}^2}$.

Once μ^2 (and thus $v_1^2 = \mu^2 H_1^2$) is reconstructed from (6), we can rewrite the original diffusion problem (3) as

$$-\nabla \cdot v_1^2 \nabla \frac{1}{u_1} = H_1, \quad \text{in } X, \qquad \frac{1}{u_1} = \frac{1}{g_1}(\mathbf{x}), \quad \text{on } \partial X. \tag{7}$$

This is an elliptic equation for $\frac{1}{u_1}$. It allows us to solve for $\frac{1}{u_1}$ stably since $g_1(\mathbf{x}) \geq \tilde{c}_0 > 0$, for some $\tilde{c}_0$, $\forall \mathbf{x} \in \partial X$. The coefficients can then be reconstructed as $\sigma = \frac{H_1}{u_1}$ and $D = \mu^2 \sigma^2$.

The vector field method is an efficient non-iterative reconstruction strategy. It reconstructs the two coefficients in (3) uniquely and stably from two well-chosen data sets, as long as the diffusion boundary value $D_{|\partial X}$ is given. However, if $D_{|\partial X}$ is not given, the vector field method can not be used. In fact, if $D_{|\partial X}$ is not known, the solution to the inverse problem is not unique when only two data sets are utilized. This can been seen from the following construction.

Lemma 2.1. *Let $(D(\mathbf{x}), \sigma(\mathbf{x}))$, $\mathbf{x} \in \bar{X}$, be a coefficient pair in model (3) that produces the set of data $\mathbf{H} \equiv (H_1, H_2)$ such that the vector field β constructed from H_1 and H_2 satisfies (**B**). Then there exists a different coefficient pair $(\tilde{D}(\mathbf{x}), \tilde{\sigma}(\mathbf{x}))$, $\mathbf{x} \in \bar{X}$, that produces the same data set $\tilde{\mathbf{H}} = \mathbf{H}$.*

Proof. We construct the new pair of coefficient, $(\tilde{D}(\mathbf{x}), \tilde{\sigma}(\mathbf{x}))$ as follows.

I. Take boundary value $(\tilde{D}_{|\partial X}, \tilde{\sigma}_{|\partial X}) \neq (D_{|\partial X}, \sigma_{|\partial X})$ such that $\tilde{\mu}_{|\partial X} \neq \mu_{|\partial X}$;

II. Solve (6) with boundary value $\tilde{\mu}_B$ $(\neq \mu_B)$ and vector field β constructed from $\mathbf{H}$;

III. Solve (7) with $\tilde{v}_1^2 = \tilde{\mu}^2 H_1^2$ for $\dfrac{1}{\tilde{u}_1}$ and construct $\tilde{\sigma} = H_1/\tilde{u}_1$ and $\tilde{D} = \tilde{\mu}^2 \tilde{\sigma}^2$.

By the construction in step III, it is clear that $\tilde{H}_1 = H_1$. We now show that $\tilde{H}_2 = H_2$ as well. Using the fact that $\tilde{H}_1 = H_1$, we first observe that $-\nabla \cdot \tilde{\mu}^2 H_1^2 \nabla \dfrac{\tilde{H}_2}{H_1} = 0$. We then conclude from Step II that $-\nabla \cdot \tilde{\mu}^2 H_1^2 \nabla \dfrac{H_2}{H_1} = 0$. Combining these two equations, we obtain

$$-\nabla \cdot \tilde{\mu}^2 H_1^2 \nabla \frac{\tilde{H}_2 - H_2}{H_1} = 0, \quad \text{in } X, \qquad \frac{\tilde{H}_2 - H_2}{H_1} = 0, \quad \text{on } \partial X. \tag{8}$$

This allows us to conclude that $\tilde{H}_2 = H_2$. □

2.2 QPAT with hybrid data

The above result shows that we need additional data to uniquely reconstruct the two coefficients in qPAT if we do not have *a priori* knowledge on the boundary values of the coefficient. Ideally, we would only need new data that allow us to reconstruct these boundary values. The new data that we introduce here are the boundary photon current data that are typically measured in diffuse optical tomography [5]:

$$J(\mathbf{x}) = -\mathbf{n} \cdot D \nabla u, \qquad \mathbf{x} \in \partial X. \tag{9}$$

With this new data, we now have both H and J to solve the inverse problem. In other words, we are combining diffuse optical tomography with photoacoustic tomography to reconstruct the diffusion and absorption coefficients of the tissue, as in [36].

We assume that the data H in (2) and data J in (9) are compatible in the sense that:

$$\int_X H(\mathbf{x})d\mathbf{x} + \int_{\partial X} J(\mathbf{x})dS(\mathbf{x}) = 0. \tag{10}$$

This compatibility condition is obtained by integrating the diffusion equation in the domain X. We can then show that with data $\{\mathbf{H}, \mathbf{J}\} = \{(H_1, H_2), (J_1, J_2)\}$, we can uniquely reconstruct the two coefficient pair (D, σ), including its boundary value. The following result is a straightforward generalization of Theorem 2.4 in [8].

Theorem 2.2. *Let (D, σ) and $(\tilde{D}, \tilde{\sigma})$ be two pairs of coefficients that satisfy the assumptions in (**A**). Denote by $(\mathbf{H}, \mathbf{J})$ and $(\tilde{\mathbf{H}}, \tilde{\mathbf{J}})$ the corresponding data sets produced by the coefficient pairs from the equation (3). Let β be the vector field constructed from $\mathbf{H}$ that starts from $\Gamma \subset \partial X$ that satisfies (**B**). Then*

$$(\mathbf{H}, \mathbf{J}) = (\tilde{\mathbf{H}}, \tilde{\mathbf{J}}) \qquad \textit{implies} \qquad (D, \sigma) = (\tilde{D}, \tilde{\sigma}). \tag{11}$$

Moreover, the following stability estimates hold:

$$\|\mu - \tilde{\mu}\|_{L^2(\partial X)} \leq C\Big(\|\mathbf{H} - \tilde{\mathbf{H}}\|_{(\mathcal{H}^1(\partial X))^2} + \|\mathbf{J} - \tilde{\mathbf{J}}\|_{(L^2(\partial X))^2}\Big), \tag{12}$$

$$\|\mu - \tilde{\mu}\|_{L^2(X)} \leq \tilde{C}\Big(\|\mathbf{H} - \tilde{\mathbf{H}}\|_{(\mathcal{H}^1(X))^2} + \|\mathbf{H} - \tilde{\mathbf{H}}\|^2_{(\mathcal{H}^1(\partial X))^2} + \|\mathbf{H} - \tilde{\mathbf{H}}\|_{(\mathcal{H}^1(\partial X))^2}\|\mathbf{J} - \tilde{\mathbf{J}}\|_{(L^2(\partial X))^2}\Big)^{\frac{1}{2}} \tag{13}$$

with C and $\tilde{C}$ two constants.

Proof. We first reconstruct the coefficients on Γ, the part of the boundary where the vector field β starts. We observe that

$$\mathbf{n} \cdot \beta_{|\Gamma} = \mathbf{n} \cdot \big[H_1^2 \nabla \frac{H_2}{H_1}\big]_{|\Gamma} = \mathbf{n} \cdot \big[H_1^2 \nabla \frac{u_2}{u_1}\big]_{|\Gamma} = \frac{H_{1|\Gamma}^2}{u_{1|\Gamma}^2}\big(u_{1|\Gamma}[\mathbf{n} \cdot \nabla u_2]_{|\Gamma} - u_{2|\Gamma}[\mathbf{n} \cdot \nabla u_1]_{|\Gamma}\big). \tag{14}$$

We now replace $[\mathbf{n} \cdot \nabla u_1]_{|\Gamma}$ by $-\frac{J_{1|\Gamma}}{D_{|\Gamma}}$ and $[\mathbf{n} \cdot \nabla u_2]_{|\Gamma}$ by $-\frac{J_{2|\Gamma}}{D_{|\Gamma}}$ in (14) to obtain

$$\mathbf{n} \cdot \beta_{|\Gamma} = \frac{H_{1|\Gamma}^2}{D_{|\Gamma} u_{1|\Gamma}^2}\big(g_{2|\Gamma} J_{1|\Gamma} - g_{1|\Gamma} J_{2|\Gamma}\big) = \frac{1}{\mu_{|\Gamma}^2}\big(g_{2|\Gamma} J_{1|\Gamma} - g_{1|\Gamma} J_{2|\Gamma}\big). \tag{15}$$

This leads to

$$\mu_{|\Gamma}^2 = \frac{1}{\mathbf{n} \cdot \beta_{|\Gamma}}\big(g_{2|\Gamma} J_{1|\Gamma} - g_{1|\Gamma} J_{2|\Gamma}\big). \tag{16}$$

Since $\mathbf{n} \cdot \beta_{|\Gamma} \leq -c_0 < 0$ for some positive c_0 on Γ, (16) allows us to reconstruct $\mu_{|\Gamma}^2$ uniquely. In fact, this formula works for any part of the boundary where $\mathbf{n} \cdot \beta \neq 0$. The uniqueness

result (11) then follows from uniqueness of solutions to the transport equation (6) and the diffusion equation (7).

The stability estimate (12) follows straightforwardly from the reconstruction formula (16). To simplify the notation, let $\nu_{|\Gamma} = \mu^2_{|\Gamma}$, $A = \big(g_{2|\Gamma} J_{1|\Gamma} - g_{1|\Gamma} J_{2|\Gamma}\big)$. We first observe that A is bounded. We then have

$$|\nu_{|\Gamma} - \tilde{\nu}_{|\tilde{\Gamma}}| = |\frac{\mathbf{n}\cdot\tilde{\beta}_{|\tilde{\Gamma}} A - \mathbf{n}\cdot\beta_{|\Gamma}\tilde{A}}{\mathbf{n}\cdot\beta_{|\Gamma}\mathbf{n}\cdot\tilde{\beta}_{|\Gamma}}| \leq C_1\Big(|A-\tilde{A}| + |\mathbf{n}\cdot(\beta_{|\Gamma} - \tilde{\beta}_{|\tilde{\Gamma}})|\Big)$$
$$\leq \tilde{C}_1\Big(|J_1 - \tilde{J}_1| + |J_2 - \tilde{J}_2| + |\beta_{|\Gamma} - \tilde{\beta}_{|\tilde{\Gamma}}|\Big). \quad (17)$$

We now check that

$$\beta - \tilde{\beta} = (H_1 - \tilde{H}_1)\nabla H_2 + \tilde{H}_1(\nabla H_2 - \nabla\tilde{H}_2) + (H_2 - \tilde{H}_2)\nabla H_1 + \tilde{H}_2(\nabla H_1 - \nabla\tilde{H}_1). \quad (18)$$

Based on the fact that $H_1, H_2 \in W^{1,\infty}(X)$, we conclude that

$$\|\beta - \tilde{\beta}\|_{L^2(X)} \leq C_2\|\mathbf{H} - \tilde{\mathbf{H}}\|_{(\mathcal{H}^1(X))^2}. \quad (19)$$

The stability estimate (12) is a direct consequence of (17) and (19).

To derive the stability estimate (13), we follow the steps in [8]. We verify that

$$0 = \nabla\cdot(\nu\beta - \tilde{\nu}\tilde{\beta}) = \nabla\cdot(\frac{\nu-\tilde{\nu}}{\nu})(\nu\beta) + \nabla\cdot\tilde{\nu}(\beta - \tilde{\beta}). \quad (20)$$

Let $\varphi(x) : \mathbb{R} \to \mathbb{R}^+$ be a function that is twice differentiable, then we check, using the fact that $\nu\beta$ and $\tilde{\nu}\tilde{\beta}$ are divergence-free vector fields and (20), that

$$\nabla\cdot\varphi(\frac{\nu-\tilde{\nu}}{\nu})(\nu\beta) + \varphi'(\frac{\nu-\tilde{\nu}}{\nu})\nabla\cdot\tilde{\nu}(\beta-\tilde{\beta}) = 0. \quad (21)$$

Let $\zeta \in \mathcal{H}^1(X)$ be a test function. We multiply the above equation by ζ and integrate by part to obtain

$$\int_{\partial X}\mathbf{n}\cdot\beta\zeta\varphi\nu dS(\mathbf{x}) - \int_X \varphi\nu\beta\cdot\nabla\zeta d\mathbf{x} + \int_{\partial X}\mathbf{n}\cdot(\beta-\tilde{\beta})\zeta\varphi'\tilde{\nu}dS(\mathbf{x})$$
$$- \int_X \varphi'\tilde{\nu}(\beta-\tilde{\beta})\cdot\nabla\zeta d\mathbf{x} - \int_X \zeta\varphi''\tilde{\nu}(\beta-\tilde{\beta})\cdot\nabla\frac{\nu-\tilde{\nu}}{\nu}d\mathbf{x} = 0. \quad (22)$$

where the arguments for φ, φ' and φ'' are all $\frac{\nu-\tilde{\nu}}{\nu}$. Taking $\zeta = \frac{H_2}{H_1}$, we obtain, after some re-arrangements,

$$\int_X \varphi\nu H_1^2|\nabla\frac{H_2}{H_1}|^2 d\mathbf{x} = \int_{\partial X}\big(\mathbf{n}\cdot H_1^2\nabla\frac{H_2}{H_1}\big)\frac{H_2}{H_1}\varphi\nu dS(\mathbf{x}) + \int_{\partial X}\mathbf{n}\cdot(\beta-\tilde{\beta})\frac{H_2}{H_1}\varphi'\tilde{\nu}dS(\mathbf{x})$$
$$- \int_X \varphi'\tilde{\nu}(\beta-\tilde{\beta})\cdot\nabla\frac{H_2}{H_1}d\mathbf{x} - \int_X \frac{H_2}{H_1}\varphi''\tilde{\nu}(\beta-\tilde{\beta})\cdot\nabla\frac{\nu-\tilde{\nu}}{\nu}d\mathbf{x}. \quad (23)$$

Now let $\varphi(x) = |x|^p$, and taking into account the fact that the first and the third terms on the right are smaller than the second and the fourth terms respectively, and that $\nabla\frac{\nu-\tilde{\nu}}{\nu}$ is bounded a.e., we arrive at

$$\|\nu-\tilde{\nu}\|^p_{L^p(X)} \leq C_3\Big(\int_{\partial X}|(\beta-\tilde{\beta})||\nu-\tilde{\nu}|^{p-1}dS(\mathbf{x}) + \int_X |\beta-\tilde{\beta}||\nu-\tilde{\nu}|^{p-2}d\mathbf{x}\Big). \tag{24}$$

Applying Hölder's inequality to the right hand side terms lead to

$$\|\nu-\tilde{\nu}\|^p_{L^p(X)} \leq \tilde{C}_3\Big(\|\beta-\tilde{\beta}\|_{L^{\frac{p}{p-1}}(\partial X)}\|\nu-\tilde{\nu}\|^{p-1}_{L^p(\partial X)} + \|\beta-\tilde{\beta}\|_{L^{\frac{p}{p-1}}(X)}\|\nu-\tilde{\nu}\|^{p-2}_{L^p(X)}\Big). \tag{25}$$

The estimate (13) then follows from (25), (12) and taking $p=2$. □

Using interpolation theory, slightly more general stability estimates can be obtained with more careful analysis as in [8].

We can now state the following result in Theorem 2.2 to the original model (1) that we are interested.

Corollary 2.3. *Let (D,σ) be a pair of coefficients in the equation (1) that satisfy the assumptions in $(\mathbf{A})$, and $(\mathbf{H},\mathbf{J})$ be the corresponding data. Assume further that the vector field β constructed from $\mathbf{H}$ satisfies $(\mathbf{B})$. Then (D,σ) is uniquely determined by $(\mathbf{H},\mathbf{J})$. Moreover, the stability estimates (12) and (13) hold.*

Proof. To reconstruct $\mu^2_{|\Gamma}$, we start again from (14). After replacing $u_{1|\Gamma}$ by $g_{1|\Gamma}+\gamma J_{1|\Gamma}$, $u_{2|\Gamma}$ by $g_{2|\Gamma}+\gamma J_{2|\Gamma}$, $[\mathbf{n}\cdot\nabla u_1]_{|\Gamma}$ by $-\frac{J_{1|\Gamma}}{D_{|\Gamma}}$, $[\mathbf{n}\cdot\nabla u_2]_{|\Gamma}$ by $-\frac{J_{2|\Gamma}}{D_{|\Gamma}}$ and some simple algebraic calculations, we obtain again (16) for the reconstruction of $\mu^2_{|\Gamma}$. The rest of the proof is identical to the proof of Theorem 2.2. □

The fact that there exists an illumination pair (g_1,g_2) such that the vector field β constructed from the data (H_1,H_2) generated with this illumination pair does not vanish, i.e., $|\beta|\geq\beta_0>0$, is not changed by the introduction of the Robin boundary condition in (1). In fact, we can easily verify as before that $\frac{u_2}{u_1}$ solves the following elliptic equation:

$$-\nabla\cdot Du_1^2\nabla\frac{u_2}{u_1}=0, \quad \text{in } X, \qquad \frac{u_2}{u_1}+\frac{\gamma}{g_1u_1}\mathbf{n}\cdot Du_1^2\nabla\frac{u_2}{u_1}=\frac{g_2}{g_1}, \quad \text{on } \partial X. \tag{26}$$

Due to the regularity and positivity assumptions on the coefficients, standard elliptic theory shows that the solutions u_1 and u_2 are positive a.e.. This means that $\frac{u_2}{u_1}$ solves (26) with again positive coefficients Du_1^2 and $\tilde{\gamma}=\dfrac{\gamma}{g_1u_1}$. The theory developed in [10] and [8, 38] thus guarantees that there exists $\frac{g_2}{g_1}$ such that $|\nabla\frac{u_2}{u_1}|>0$. For instance, in two-dimensional case, if $\frac{g_2}{g_1}$ has exactly one maximum and one minimum (i.e. it is "almost two-to-one" [38]), then $|\nabla\frac{u_2}{u_1}|\geq\alpha_0>0$ for some positive α_0.

2.3 The generalized vector field method

We are now ready to generalize the vector field method to the diffusion model (1) with data (2) and (9).

Step I. In the first step, solve the transport equation (5) for μ^2. The boundary value of μ^2 is constructed according to (16):

$$\begin{aligned} &\nabla \cdot \mu^2 \beta = 0, && \text{in } X, \\ &\mu^2 = \frac{1}{\mathbf{n} \cdot \beta_{|\Gamma}} \big(g_{2|\Gamma} J_{1|\Gamma} - g_{1|\Gamma} J_{2|\Gamma} \big), && \text{on } \Gamma. \end{aligned} \tag{27}$$

Step II. In the second step of the vector field method, we solve a modified version of the diffusion problem (7):

$$-\nabla \cdot v_1^2 \nabla \frac{1}{u_1} = H_1, \quad \text{in } X, \qquad \frac{1}{u_1} = \frac{1}{g_1 + \gamma J_1}, \quad \text{on } \partial X \tag{28}$$

where as before, $v_1^2 = \mu^2 H_1^2 = (\sqrt{D} u_1)^2$. This elliptic equation is well-posed as long as $g_1 + \gamma J_1 \neq 0$. In practice, due to the noise presented in the data J_1, we might run into the situation that $g_1 + \gamma J_1 = 0$. Thus we might run into problems when solving (28). We thus regularize the problem as follows

$$\frac{1}{u_1}(\mathbf{x}) = \begin{cases} \dfrac{1}{g_1 + \gamma J_1}, & g_1 + \gamma J_1 \neq 0 \\ \dfrac{1}{g_1 + \gamma J_1 + \varepsilon}, & g_1 + \gamma J_1 = 0 \end{cases} \tag{29}$$

where ε is a small regularization constant.

Step $\widetilde{\text{II}}$. There is an alternative reconstruction strategy for the second step of the generalized vector field method. To derive the strategy, let us assume that the diffusion coefficient is regular enough, say $D(\mathbf{x}) \in W^{2,\infty}(X)$. We can then perform the Liouville transform $v_1 = \sqrt{D} u_1$ to obtain the following identity

$$q \equiv \frac{\Delta \sqrt{D}}{\sqrt{D}} + \frac{1}{\mu \sqrt{D}} = -\frac{\Delta v_1}{v_1}. \tag{30}$$

The quantity v_1 is already reconstructed from the first step of the vector field method. We can thus compute $\dfrac{\Delta v_1}{v_1}$ to obtain q. This is equivalent to say that we can reconstruct the quantity q from the first step of the vector field method. The above identity can be slightly rewritten to obtain the following elliptic equation for $\sqrt{D}$:

$$\Delta \sqrt{D} - q \sqrt{D} + \frac{1}{\mu} = 0, \quad \text{in } X, \qquad \sqrt{D} = \sqrt{D_{|\partial X}}, \quad \text{on } \partial X. \tag{31}$$

With $\sqrt{D_{|\partial X}}$ reconstructed already (since $\mu_{|\partial X}$ and $\sigma_{|\partial X}$ are reconstructed already), we can solve this elliptic PDE for $\sqrt{D}$. Note that this reconstruction strategy contains regularization effect. If the true diffusion coefficient D contains discontinuities, for instance, then these

discontinuities would have been regularized in the reconstruction since (31) would not allow discontinuous solutions. Moreover, to compute $q = -\frac{\Delta v_1}{\sqrt{v_1}}$, we have to compute Δv_1. Since v_1 might not be smooth enough, we would not have to regularize it as well. To do that, we convolve v_1 with a Gaussian kernel φ to get $\Phi(v_1) = \int_X \varphi(\mathbf{x}-\mathbf{y})v_1(\mathbf{y})d\mathbf{y}$. We control the strength of the regularization by adjusting the variance of the Gaussian kernel. We then compute q as $q = -\frac{\Delta\Phi(v_1)}{v_1}$.

3 The full nonlinear reconstruction algorithm

Provided that the denominator $\mathbf{n}\cdot\beta_{|\Gamma} \neq 0$ in (27) and the denominator $g_{1|\Gamma} + \gamma J_{1|\Gamma} \neq 0$ in (28), the generalized vector field method can be applied to solve the inverse problem to get unique and stable reconstructions of the diffusion and absorption coefficients, inside the domain and on the boundary. In practical situations, however, both denominators can vanish on part of the boundary due to the presence of measurement noise. In this type of situations, regularization strategies such as those mentioned in the previous section have to be employed in order to use the vector field method.

We now present an optimization-based iterative method to deal with this complication. We intend to use the efficient vector field method in the new iterative method whenever it could be used. Our idea is to separate the unknown coefficients in the interior of the domain from their values on the boundary of the domain. As we have seen from the previous section, in each iteration, once the values on the boundary are updated, we can have the vector field reconstruction method to update the interior values, by solving only a transport equation and a diffusion equation. The benefit of this hybrid reconstruction lies in the fact that it reduces the number of unknowns in the system so that we only need to deal with this reduced system.

To set up the optimization algorithm, let us denote by $D_I = D_{|X}$ (resp. $\sigma_I = \sigma_{|X}$) and $D_B = D_{|\partial X}$ (resp. $\sigma_B = \sigma_{|\partial X}$) the value of the diffusion (absorption) coefficient on the interior and boundary of the domain respectively. To make a connection with the vector field method, we now work on the coefficient pair (μ, D) instead of (σ, D). We denote by μ_I and μ_B the interior and boundary values of μ respectively. We are now ready to write down the interior and boundary data abstractly into the following form

$$\begin{aligned} H_{|X} &= \sigma_I u_I = \frac{1}{\mu_I}\sqrt{D_I}u_I \equiv H_{|X}(\mu_I, \mu_B, D_I, D_B), \\ H_{|\partial X} &= \sigma_B u_B = \frac{1}{\mu_B}\sqrt{D_B}u_B \equiv H_{|\partial X}(\mu_I, \mu_B, D_I, D_B), \\ J &= -\mathbf{n}\cdot D_B\nabla u \equiv J(\mu_I, \mu_B, D_I, D_B). \end{aligned} \tag{32}$$

Our method is to eliminate the variables μ_I and D_I because they are determined uniquely by the value of μ_B and D_B according to the vector field method. Let $\mathbf{F}$ be the map $(\mu_I, D_I) = \mathbf{F}(\mu_B, D_B)$, and G be the map $\mathbf{n}\cdot\nabla u = G(\mu_B, D_B)$, then we can write the data as

$$\begin{aligned} H_{|X}(\mu_B, D_B) &= H_{|X}(\mathbf{F}(\mu_B, D_B), \mu_B, D_B), \\ H_{|\partial X}(\mu_B, D_B) &= H_{|\partial X}(\mathbf{F}(\mu_B, D_B), \mu_B, D_B), \\ J(\mu_B, D_B) &= J(G(\mu_B, D_B), \mu_B, D_B). \end{aligned} \tag{33}$$

We have thus built the (implicit) map from the unknown (μ_B, D_B) to our given data $(H_{|X}, H_{|\partial X}, J)$. The objective now is to invert this map to recover (μ_B, D_B).

In practice, we have data $(H_{|X}, H_{|\partial X}, J)$ constructed from $K \geq 2$ different illuminations. We also have to deal with data that contain noise or inconsistency in the measurements. It is thus natural to solve the nonlinear system with some proper regularization term. Here we simply use least-square. Other choices can be done in the same way. Denote by Π the space of admissible coefficients (μ_B, D_B), then we solve the following nonlinear least-square minimization problem

$$\min_{(\mu_B, D_B)\in\Pi} \mathcal{O}(\mu_B, D_B). \tag{34}$$

where the objective functional $\mathcal{O} : \Pi \to \mathbb{R}$ is defined as

$$\min_{\mu_B, D_B} \mathcal{O}(\mu_B, D_B) = \frac{1}{2}\sum_{k=1}^{K-1} \widehat{\mathcal{O}}_k(\mu_B, D_B) + \frac{1}{2}\sum_{k=1}^{K} \widetilde{\mathcal{O}}_k(\mu_B, D_B) + \tau\mathcal{R}(\mu_B, D_B) \tag{35}$$

with the components of objective functional given by

$$\widehat{\mathcal{O}}_k(\mu_B, D_B) = \|H_{k|X}(\mathbf{F}_k(\mu_B, D_B), \mu_B, D_B) - H^*_{k|X}\|^2_{L^2(X)} + \|H_{k|\partial X} - H^*_{k|\partial X}\|^2_{L^2(\partial X)}, \tag{36}$$

$$\widetilde{\mathcal{O}}_k(\mu_B, D_B) = \|J_k(G_k(\mu_B, D_B), \mu_B, D_B) - J^*_k\|^2_{L^2(\partial X)}. \tag{37}$$

The regularization term $\mathcal{R}$, with strength τ, is used to regularize the unknowns when noisy data are utilized. Note that the summation in the first term in the objective functional (35) is over $K-1$, not K, terms. This is due to the fact that we can only construct $K-1$ vector fields out of K sets of data H. We denote by $\beta_k = H_k^2\nabla\frac{H_K}{H_k}$ the k-th vector field.

We solve the minimization problem by a quasi-Newton method with the BFGS updating rule on the Hessian operator [12, 29, 40, 43]. This method requires the Fréchet derivatives of the functional $\mathcal{O}$ with respect to the unknowns μ_B and D_B. These derivatives can be computed using the adjoint state method and the chain rule. Let us denote by $\mathcal{D}_{\mu_B}\mathcal{O}(\mu_B, D_B)$ (resp. $\mathcal{D}_{D_B}\mathcal{O}(\mu_B, D_B)$), or simply $\mathcal{D}_{\mu_B}\mathcal{O}$ (resp. $\mathcal{D}_{D_B}\mathcal{O}$), the partial Fréchet derivative of $\mathcal{O}$ with respect to μ_B (resp. D_B) evaluated at (μ_B, D_B). Then the chain rule implies that $\mathcal{D}_{\mu_B}\mathcal{O}(\mu_B, D_B)\hat{\mu}_B$, $\hat{\mu}_B$ being the perturbation to μ_B, can be computed as

$$\mathcal{D}_{\mu_B}\mathcal{O}\hat{\mu}_B = \frac{1}{2}\sum_{k=1}^{K-1}\Big[\mathcal{D}_{\mu_B}\widehat{\mathcal{O}}_k\hat{\mu}_B + \mathcal{D}_{\mathbf{F}_k}\widehat{\mathcal{O}}_k \circ \mathcal{D}_{\mu_B}\mathbf{F}_k\hat{\mu}_B\Big] + \frac{1}{2}\sum_{k=1}^{K}\Big[\mathcal{D}_{\mu_B}\widetilde{\mathcal{O}}_k\hat{\mu}_B + \mathcal{D}_G\widetilde{\mathcal{O}}_k \circ \mathcal{D}_{\mu_B}G\hat{D}_B\Big] + \tau\mathcal{D}_{\mu_B}\mathcal{R}\hat{\mu}_B. \tag{38}$$

To obtain explicit expression for this quantity, let us introduce w_k, the solution of the following adjoint, with respect to (28), equation:

$$-\nabla\cdot\mu^2H_k^2\nabla w_k = \nabla\cdot 2\mu H_k^2\nabla\frac{1}{u_k}, \quad \text{in } X, \qquad w_k = 0, \quad \text{on } \partial X, \tag{39}$$

and $\tilde{w}_k$, the solution of the following adjoint, with respect to (27), equation:

$$-2\mu\beta_k\cdot\nabla\tilde{w}_k = -\frac{\sqrt{D_I}}{\mu_I}u_k\big(u_kw_k + \frac{1}{\mu_I}\big)(H_k - H_k^*), \quad \text{in } X, \qquad \tilde{w}_k(\mathbf{x}) = 0, \quad \text{on } \partial X\backslash\Gamma_k \tag{40}$$

with Γ_k being the part of the boundary where the k-th vector field, β_k, starts, and thus $\partial X \backslash \Gamma_k$ the part of the boundary where β_k ends. We can then show by straightforward calculations that

$$\mathcal{D}_{\mu_B}\mathcal{O}\hat{\mu}_B = \sum_{k=1}^{K-1}\langle -\frac{(g_k+\gamma J_k^*)\sqrt{D_B}}{\mu_B^2}\hat{\mu}_B, H_{k|\partial X} - H^*_{k|\partial X}\rangle_{L^2(\partial X)} - \langle 2\mathbf{n}\cdot\beta\mu\tilde{w}_k, \hat{\mu}_B\rangle_{L^2(\Gamma)} + \sum_{k=1}^{K}\langle D_B(g_k+\gamma J_k)^2\mathbf{n}\cdot\nabla w_k\hat{\mu}_B, J_k - J_k^*\rangle_{L^2(\partial X)} + \tau\mathcal{D}_{\mu_B}\mathcal{R}\hat{\mu}_B. \quad (41)$$

where $\langle\cdot,\cdot\rangle_{L^2(\mathcal{X})}$ denotes the inner product in $L^2(\mathcal{X})$.

The derivative with respect to D_B can be computed in the same manner. In fact, we can show that

$$\mathcal{D}_{D_B}\mathcal{O}\hat{D}_B = \sum_{k=1}^{K-1}\langle \frac{(g_k+\gamma J_k)}{2\mu_B\sqrt{D_B}}\hat{D}_B, H_{k|\partial X} - H^*_{k|\partial X}\rangle_{L^2(\partial X)} + \sum_{k=1}^{K}\langle -\mathbf{n}\cdot\nabla u_k\hat{D}_B, J_k - J_k^*\rangle_{L^2(\partial X)} + \tau\mathcal{D}_{D_B}\mathcal{R}\hat{D}_B. \quad (42)$$

We are ready to introduce the BFGS quasi-Newton method [28, 40] for the hybrid reconstruction strategy. We denote by η the column vector that contains the discretized values of the unknowns $(\mu_B, D_B)^t$, $\mathfrak{g}$ the discretized version the Fréchet derivatives $(\mathcal{D}_{\mu_B}\mathcal{O}, \mathcal{D}_{D_B}\mathcal{O})$, and $\mathfrak{H}$ the inverse Hessian matrix. Assume that we have the inverse Hessian matrix at iteration j, then the BFGS quasi-Newton method updates the inverse Hessian matrix for iteration $j+1$ according to the rule:

$$\mathfrak{H}_j = W_{j-1}^t\mathfrak{H}_{j-1}W_{j-1} + \rho_{j-1}s_{j-1}s_{j-1}^t \quad (43)$$

with $W_{j-1} = \mathfrak{I} - \rho_{j-1}y_{j-1}s_{j-1}^t$, $s_{j-1} = \eta_j - \eta_{j-1}$, $y_{j-1} = \mathfrak{g}_j - \mathfrak{g}_{j-1}$, and $\rho_{j-1} = \frac{1}{y_{j-1}^t s_{j-1}}$, $\mathfrak{I}$ being the identity matrix. The whole algorithm now proceeds as follows.

Hybrid Quasi-Newton Algorithm.

S1. Set $j=0$, initial guess $\eta_0 = (\mu_B^0, D_B^0)$, $\mathfrak{H}_0 = \mathfrak{I}$;

S2. Solve the equations (27), (28), (39) and (40) with η_j for $1 \le k \le K-1$; calculate the Fréchet derivative $\mathfrak{g}_j$ according to (41) and (42);

S3. If $j \ge 1$, update the inverse Hessian matrix according to (43);

S4. Update the unknown $\eta_{j+1} = \eta_j + \alpha\mathfrak{H}_j\mathfrak{g}_j$, with α determined by a line search algorithm;

S5. If stopping criteria satisfied, stop; otherwise, set $j = j+1$ and go to S2;

We refer interested readers to [28, 40] for more details on the BFGS algorithms, and to reference [29, 43] for applications of those algorithms to optical tomographic problems. The implementation we employed here is adapted from the code that we developed in [43]. We

observe in numerical simulations, see those presented in Section 5 that the algorithm converges very fast and it converges for initial guesses that are very far from the true coefficients. This is not surprising since the inverse problem in qPAT is well-posed as we see from the previous section.

4 The linearized reconstruction algorithm

We now consider the linearization of the nonlinear inverse problem by Born approximation. We assume again that we have data for K illumination sources $\{g_k\}_{k=1}^K$ and we denote by u_k the solution to the diffusion problem with coefficients (D, σ) and source g_k.

We linearize around some *known*, but not necessarily constant, background optical properties $D_0(\mathbf{x}) > 0$ and $\sigma_0(\mathbf{x}) > 0$. To be more precise, we assume

$$D(\mathbf{x}) = D_0(\mathbf{x}) + \tilde{D}(\mathbf{x}), \qquad \sigma(\mathbf{x}) = \sigma_0(\mathbf{x}) + \tilde{\sigma}(\mathbf{x}), \quad \mathbf{x} \in \bar{X} \tag{44}$$

where the perturbations are small in the sense that $\|\frac{\tilde{\sigma}(\mathbf{x})}{\sigma_0}\|_{L^\infty} \ll 1$ and $\|\frac{\tilde{D}(\mathbf{x})}{D_0}\|_{L^\infty} \ll 1$. The corresponding perturbation to the quantity μ and μ^2 are thus given, to the first order, by

$$\mu = \frac{\sqrt{D_0}}{\sigma_0} - \frac{\sqrt{D_0}}{\sigma_0^2}\tilde{\sigma} + \frac{1}{2}\frac{1}{\sqrt{D_0}\sigma_0}\tilde{D} \equiv \mu_0 + \tilde{\mu}, \qquad \text{and} \qquad \mu^2 = \mu_0^2 + 2\mu_0\tilde{\mu} \tag{45}$$

respectively. These can be verified by simple Taylor expansions.

Let us denote by $U_k(\mathbf{x})$ the solution to the diffusion problem with the known background coefficients (D_0, σ_0) and source g_k. Then (44) implies that the solution u_k of the diffusion problem with coefficients (D, σ) can be formally written as

$$u_k(\mathbf{x}, \mathbf{v}) = U_k(\mathbf{x}) + \tilde{u}_k(\mathbf{x}), \tag{46}$$

with $\tilde{u}_k(\mathbf{x})$ the perturbation in the solution caused by the perturbations in the coefficients.

The perturbations in (44) and (46) imply that the interior data $H_{k|X}$ and the boundary data $H_{k|\partial X}$ and J_k are now given respectively, to the first order, by

$$H_{k|X}(\mathbf{x}) = \sigma_{0|X}U_{k|X} + \frac{\sigma_{0|X}}{2D_{0|X}}U_{k|X}\tilde{D}_{|X} - \frac{\sigma_{0|X}}{\mu_{0|X}}U_{k|X}\tilde{\mu}_{|X} + \sigma_{0|X}\tilde{u}_{k|X}, \tag{47}$$

$$H_{k|\partial X}(\mathbf{x}) = \sigma_{0|\partial X}U_{k|\partial X} + \frac{\sigma_{0|\partial X}}{2D_{0|\partial X}}U_{k|\partial X}\tilde{D}_{|\partial X} - \frac{\sigma_{0|\partial X}}{\mu_{0|\partial X}}U_{k|\partial X}\tilde{\mu}_{|\partial X}, \tag{48}$$

$$J_k(\mathbf{x}) = -D_0\mathbf{n}\cdot\nabla U_k - \tilde{D}\mathbf{n}\cdot\nabla U_k - D_0\mathbf{n}\cdot\nabla\tilde{u}_k \tag{49}$$

where we have replaced $\dfrac{\sqrt{D_0}}{\mu_0}$ by σ_0.

It is straightforward to verify, using the transport equation (27), that the equation satisfied by the perturbation $\tilde{\mu}$, for vector field β_k, $1 \le k \le K-1$, is

$$\nabla\cdot 2\mu_0\tilde{\mu}\beta_k = 0, \quad \text{in} \quad X, \qquad \tilde{\mu} = \tilde{\mu}_B, \quad \text{on} \quad \Gamma_k. \tag{50}$$

and the equation satisfied by the perturbation $\tilde{u}_k(\mathbf{x})$, to the first order, is

$$-\nabla\cdot\mu_0^2 H_k^2\nabla\frac{\tilde{u}_k}{U_k^2}=\nabla\cdot 2\mu_0\tilde{\mu}\frac{H_k^2}{U_k^2}\nabla U_k,\quad \text{in } X,\qquad \frac{\tilde{u}_k}{U_k^2}=0,\quad \text{on } \partial X. \tag{51}$$

It can then be shown, using the fact that u_k is Fréchet differentiable, that the terms omitted are indeed high order terms; see for instance [27, Lemma 4.5.1].

Let us denote by G_k^t the solution of the adjoint transport problem

$$-2\mu_0\beta_k\cdot\nabla G_k^t(\mathbf{x};\mathbf{y})=\delta(\mathbf{x}-\mathbf{y}),\quad \text{in } X,\qquad G_k^t(\mathbf{x};\mathbf{y})=0,\quad \text{on } \partial X\backslash\Gamma_k \tag{52}$$

with $\delta(\mathbf{x}-\mathbf{y})$ being the usual Dirac delta function. Then the solution of (50) is given by

$$\tilde{\mu}(\mathbf{x})=-\int_{\Gamma_k}2\mu_0(\mathbf{y})G_k^t(\mathbf{y};\mathbf{x})\tilde{\mu}_B(\mathbf{y})dS(\mathbf{y}),\quad \mathbf{x}\in X. \tag{53}$$

We now introduce the volume and boundary Green's functions $G_k^v(\mathbf{x};\mathbf{y})$ and $G_k^b(\mathbf{x};\mathbf{y})$ for the diffusion problem with background optical properties, the solutions of the diffusion equations

$$-\nabla\cdot\mu_0^2 H_k^2\nabla G_k^v(\mathbf{x};\mathbf{y})=\delta(\mathbf{x}-\mathbf{y}),\quad \text{in } X,\qquad G_k^v(\mathbf{x};\mathbf{y})=0,\quad \text{on } \partial X. \tag{54}$$

and

$$-\nabla\cdot\mu_0^2 H_k^2\nabla G_k^b(\mathbf{x};\mathbf{y})=0,\quad \text{in } X,\qquad G_k^b(\mathbf{x};\mathbf{y})=\delta(\mathbf{x}-\mathbf{y}),\quad \text{on } \partial X. \tag{55}$$

respectively. Then we can now show, using (51), (54), (55) and some simple integration by parts, that

$$\frac{\tilde{u}_k}{U_k^2}(\mathbf{x})=-\int_X 2\mu_0(\mathbf{y})\frac{H_k^2}{U_k^2}\nabla U_k\cdot\nabla G_k^v(\mathbf{y};\mathbf{x})\tilde{\mu}(\mathbf{y})d\mathbf{y},\quad \mathbf{x}\in X \tag{56}$$

and

$$-D_0\mathbf{n}\cdot\nabla\tilde{u}_k=2\mu_0\tilde{\mu}\frac{H_k^2}{U_k^2}\mathbf{n}\cdot\nabla U_k-\int_X 2\mu_0(\mathbf{y})\frac{H_k^2}{U_k^2}\nabla U_k(\mathbf{y})\cdot\nabla G_k^b(\mathbf{y};\mathbf{x})\tilde{\mu}(\mathbf{y})d\mathbf{y},\quad \mathbf{x}\in\partial X. \tag{57}$$

Combining (56) and (57) with (47) and (49), we can show that

$$\tilde{H}_{k|X} \equiv H_{k|X}-\sigma_{0|X}U_{k|X}=\mathscr{M}_{k|X}\tilde{\mu}_I+\sigma_{0|X}U_{k|X}^2\mathscr{L}_k^v\tilde{\mu}_I+\mathscr{N}_{k|X}\tilde{D}_I, \tag{58}$$

$$\tilde{H}_{k|\partial X} \equiv H_{k|\partial X}-\sigma_{0|\partial X}U_{k|\partial X}=\mathscr{M}_{k|\partial X}\tilde{\mu}_B+\mathscr{N}_{k|\partial X}\tilde{D}_B, \tag{59}$$

$$\tilde{J}_k \equiv J_k+D_0\mathbf{n}\cdot\nabla U_k=\mathscr{L}_k^b\tilde{\mu}_I+\mathscr{P}_k\tilde{\mu}_B+\mathscr{Q}_k\tilde{D}_B \tag{60}$$

where to simplify the presentation, we have defined the operators:

$$\mathscr{M}_{k|X}\tilde{\mu}_I=-\frac{\sigma_{0|X}U_k}{\mu_{0|X}}\tilde{\mu}_I,\qquad \mathscr{N}_{k|X}\tilde{D}_I=\frac{\sigma_{0|X}U_k}{2D_{0|X}}\tilde{D}_I \tag{61}$$

$$\mathscr{M}_{k|\partial X}\tilde{\mu}_B=-\frac{\sigma_{0|\partial X}(g_k+\gamma J_k^*)}{\mu_{0|\partial X}}\tilde{\mu}_B,\qquad \mathscr{N}_{k|\partial X}\tilde{D}_B=\frac{\sigma_{0|\partial X}(g_k+\gamma J_k^*)}{2\sqrt{D_{0|\partial X}}}\tilde{D}_B \tag{62}$$

$$\mathscr{P}_k\tilde{\mu}_B=2\mu_{0|\partial X}\frac{H_{k|\partial X}^2}{U_{k|\partial X}^2}\mathbf{n}\cdot\nabla U_k\tilde{\mu}_B,\qquad \mathscr{Q}_k\tilde{D}_B=-\mathbf{n}\cdot\nabla U_k\tilde{D}_B \tag{63}$$

$$\mathscr{L}_k^t \tilde{\mu}_B = -\int_{\Gamma_k} 2\mu_0(\mathbf{y}) G_k^t(\mathbf{y};\mathbf{x}) \tilde{\mu}_B(\mathbf{y}) d\mathbf{y} \tag{64}$$

$$\mathscr{L}_k^z \tilde{\mu}_I = -\int_X 2\mu_0 \tilde{\mu}_I(\mathbf{x}) \frac{H_k^2}{U_k^2} \nabla U_k(\mathbf{y}) \cdot \nabla G_k^z(\mathbf{y};\mathbf{x}) d\mathbf{y}, \qquad z \in \{v, b\}. \tag{65}$$

Equations (53), (58), (59) and (60) are linear integral equations for the variables ($\tilde{\mu}_I$, $\tilde{D}_I$, $\tilde{\mu}_B$, $\tilde{D}_B$). The kernels for the operators are known since they only involve the solutions of the diffusion equation and the Green functions with background optical properties μ_0 and D_0. It remains to solve these integral equations to reconstruct the unknowns ($\tilde{\mu}_I$, $\tilde{D}_I$, $\tilde{\mu}_B$, $\tilde{D}_B$), and then the real coefficients.

Let us arrange the linear maps into the following system of equations for the unknowns

$$\begin{pmatrix} \mathcal{I} & 0 & \mathscr{L}_k^t & 0 \\ \mathscr{M}_{k|X} + \sigma_{0|X} U_{k|X}^2 \mathscr{L}_k^v & \mathscr{N}_{k|X} & 0 & 0 \\ \mathscr{L}_k^b & 0 & \mathscr{P}_k & \mathscr{Q}_k \\ 0 & 0 & \mathscr{M}_{k|\partial X} & \mathscr{N}_{k|\partial X} \end{pmatrix} \begin{pmatrix} \tilde{\mu}_I \\ \tilde{D}_I \\ \tilde{\mu}_B \\ \tilde{D}_B \end{pmatrix} = \begin{pmatrix} 0 \\ \tilde{H}_{k|X} \\ J \\ \tilde{H}_{k|\partial X} \end{pmatrix} \tag{66}$$

Then we can perform a Gauss elimination to eliminate the unknowns (μ_I, D_I) to obtain

$$\begin{aligned} \left[\begin{pmatrix} \mathscr{P}_k & \mathscr{Q}_k \\ \mathscr{M}_{k|\partial X} & \mathscr{N}_{k|\partial X} \end{pmatrix} - \begin{pmatrix} \mathscr{L}_k^b & 0 \\ 0 & 0 \end{pmatrix} \begin{pmatrix} \mathcal{I} & 0 \\ \mathscr{M}_{k|X} + \sigma_{0|X} U_{k|X}^2 \mathscr{L}_k^v & \mathscr{N}_{k|X} \end{pmatrix}^{-1} \begin{pmatrix} \mathscr{L}_k^b & 0 \\ 0 & 0 \end{pmatrix} \right] \begin{pmatrix} \mu_B \\ D_B \end{pmatrix} \\ = \begin{pmatrix} 0 \\ \tilde{H}_{k|X} \end{pmatrix} - \begin{pmatrix} \mathscr{L}_k^b & 0 \\ 0 & 0 \end{pmatrix} \begin{pmatrix} \mathcal{I} & 0 \\ \mathscr{M}_{k|X} + \sigma_{0|X} U_{k|X}^2 \mathscr{L}_k^v & \mathscr{N}_{k|X} \end{pmatrix}^{-1} \begin{pmatrix} J \\ \tilde{H}_{k|\partial X} \end{pmatrix} \end{aligned} \tag{67}$$

where, following a straightforward block Gauss elimination, we have

$$\begin{pmatrix} \mathcal{I} & 0 \\ \mathscr{M}_{k|X} + \sigma_{0|X} U_{k|X}^2 \mathscr{L}_k^v & \mathscr{N}_{k|X} \end{pmatrix}^{-1} = \begin{pmatrix} \mathcal{I} & 0 \\ \mathscr{N}_{k|X}^{-1} \left(\mathscr{M}_{k|X} + \sigma_{0|X} U_{k|X}^2 \mathscr{L}_k^v \right) & \mathscr{N}_{k|X}^{-1} \end{pmatrix}. \tag{68}$$

This indicates that in order to formulate the reduced system of equations for the unknown (μ_B, D_B), we only need to invert $\mathscr{N}_{k|X}$ which can be done analytically since $\mathscr{N}_{k|X}$ is a diagonal matrix after discretization.

The system (67) is the linear system of equations that we intend to solve for the unknowns (μ_B, D_B). We collect this system for K different data sets to get an over-determined system and then solve the system in regularized linear least-square form.

5 Numerical experiments

We now present some numerical simulations based on the algorithms we have presented in the previous sections. The data used are synthetic data that are created by solving the diffusion problem (1) on a triangular mesh that is different from the Cartesian mesh we used in solving the inverse problem. The data are then interpolated to the inversion mesh using the MATLAB interpolation function `tri2grid`. It is clear that data created this way contain noise inherited from the interpolation algorithm, even though the interpolation error

is very small (since forward solutions are computed on very fine meshes). In the presentation below, we will call this type of data the "clean data" or "noiseless" data. We reserve the term "noisy data" for those data in which we added additional additive noise (uniformly distributed). The level of noise will be specified later.

To simplify the computation, we present only two-dimensional simulations. The domain we take is the square $X = (0,\ 2) \times (0,\ 2)$. We cover the domain, together with its boundary, by a fine finite element mesh of 40257 nodes and 79872 triangle elements. The results that are shown below, however, are the original results interpolated on a 81×81 grid for the convenience of plot in MATLAB. In the presentation below, we would use both $\mathbf{x}$ and (x, y) to denote a point in $\mathbb{R}^2$.

Experiment 1. In the first numerical example, we show the reconstruction of the coefficients (D, σ) from four sets of internal and boundary data. The illuminations are taken such that they are positive everywhere on the boundary. Let us denote by ∂X_b, ∂X_r, ∂X_t and ∂X_l the bottom, right, top and left parts of the boundary respectively. Then the four illuminations are give as

$$g_1(\mathbf{x}) = \begin{cases} 2, & \mathbf{x} \in \partial X_b \\ 1, & \text{otherwise} \end{cases}, \qquad g_2(\mathbf{x}) = \begin{cases} 3, & \mathbf{x} \in \partial X_r \\ 1, & \text{otherwise} \end{cases}, \qquad g_3(\mathbf{x}) = \begin{cases} 4, & \mathbf{x} \in \partial X_t \\ 1, & \text{otherwise} \end{cases}$$

and $g_4(\mathbf{x}) = 1$, $\mathbf{x} \in \partial X$. The coefficients are given by

$$D(\mathbf{x}) = 0.03 + 0.01 \sin(\pi y), \qquad \sigma(\mathbf{x}) = 0.2 + 0.1 \sin(2\pi x) \sin(2\pi y). \tag{69}$$

We performed two sets of reconstructions using noiseless and noisy synthetic data respectively. For the noisy data, we added 5% additive random noise to the data by simply multiplying each datum by $(1 + 0.05\ \texttt{random})$ with `random` a uniformly distributed random variable taking values in $[-1,\ 1]$.

The results of the reconstructions are shown in Fig. 1. The relative error, i.e. the difference between the reconstructed coefficient and the true coefficient divided by the true coefficient, in the reconstructions are shown in the bottom right plots of Fig. 1 for the case of noisy data. To look at the result of the reconstructions on the boundary values of the coefficients, we plot in Fig. 2 the reconstruction of the coefficients on the boundary of the domain. We show in Fig. 2 also the three vector fields β_k $(k = 1, 2, 3)$ constructed from the four noiseless data sets. Γ_k, the part of the boundary where β_k starts, covers 3/4 of the boundary. $\Gamma_1 \cup \Gamma_2 \cup \Gamma_3$, however, covers the whole boundary of the domain. That is the reason why boundary values are recovered on the whole boundary.

Experiment 2. We now repeat the numerical Experiment 1 by using illuminations that are only non-zero on one side of the domain. More precisely,

$$g_1 = \begin{cases} 1, & \mathbf{x} \in \partial X_b \\ 0, & \mathbf{x} \notin \partial X_b \end{cases}, \ g_2 = \begin{cases} 2, & \mathbf{x} \in \partial X_r \\ 0, & \mathbf{x} \notin \partial X_r \end{cases}, \ g_3 = \begin{cases} 3, & \mathbf{x} \in \partial X_t \\ 0, & \mathbf{x} \notin \partial X_t \end{cases}, \ g_4 = \begin{cases} 4, & \mathbf{x} \in \partial X_l \\ 0, & \mathbf{x} \notin \partial X_l \end{cases}$$

The results of the reconstruction are shown in Fig. 3. We observe that the quality of the reconstructions is very similar to that of the reconstructions in Experiment 1 as can be seen

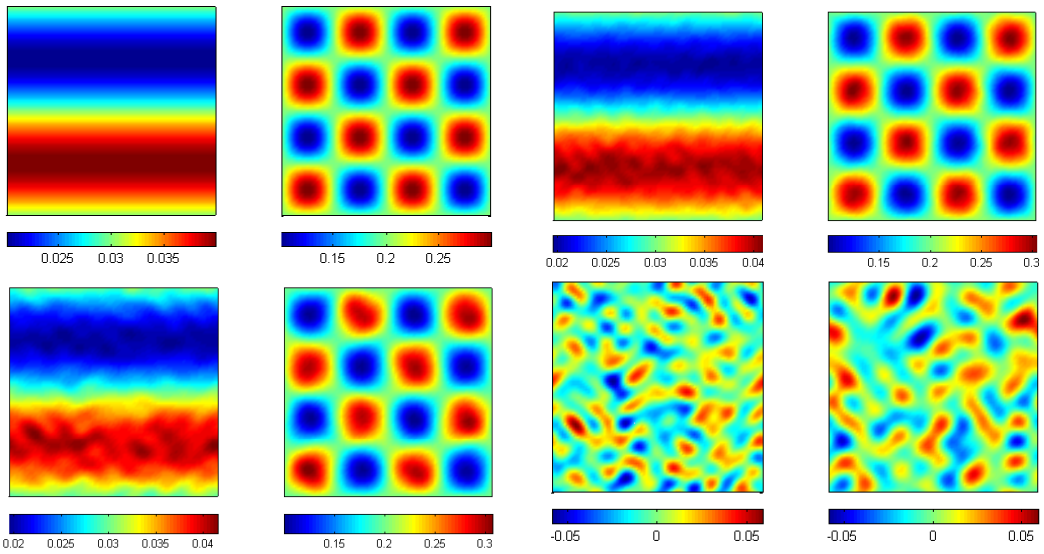

Figure 1: Reconstruction of smooth diffusion and absorption coefficients in Experiment 1. Show are real coefficients (top left), reconstructions with noiseless (top right) and noisy (bottom left) data, and the relative difference between noisy reconstruction and the true coefficients (bottom right).

from the relative errors in the reconstructions shown in the bottom right plots of Fig. 3, even though the vector fields constructed in this case are a little bit different from those in Experiment 1.

Experiment 3. In this numerical example, we attempt to reconstruct coefficients with discontinuities. To simplify the implementation, we only consider piecewise constant coefficients. The true coefficients are taken as suppositions of constant backgrounds with inclusions, as shown in the top left plots of Fig. 4. Reconstructions with both noiseless and noisy data are performed. The results have similar quality as those in the smooth coefficient cases in Experiment 1 and Experiment 2. The relative errors (in the noisy data case) are shown in the bottom right plots of Fig. 4. It is very clear that the error in the reconstruction is larger on the discontinuities then in the rest of the domain. This is mainly due to the regularization effect of our algorithm.

Experiment 4. We have seen from previous numerical simulations that the reconstruction of both smooth and piecewise constant coefficients are very accurate. The results are similar to those presented in [8, 9]. The results are all reconstructed with illuminations on all sides of the boundary. In this simulation, we present some reconstructions with data collected only on one side of the boundary. We still use four illuminations. They are given as

$$g_1(\mathbf{x}) = \begin{cases} 1+y, & \mathbf{x} \in \partial X_L \\ 0, & \text{otherwise} \end{cases}, \qquad g_2(\mathbf{x}) = \begin{cases} 3-y, & \mathbf{x} \in \partial X_L \\ 0, & \text{otherwise} \end{cases}$$

$$g_3(\mathbf{x}) = \begin{cases} 1+\sin\dfrac{\pi y}{2}, & \mathbf{x} \in \partial X_L \\ 0, & \text{otherwise} \end{cases}, \qquad g_4(\mathbf{x}) = \begin{cases} 1, & \mathbf{x} \in \partial X_L \\ 0, & \text{otherwise} \end{cases}$$

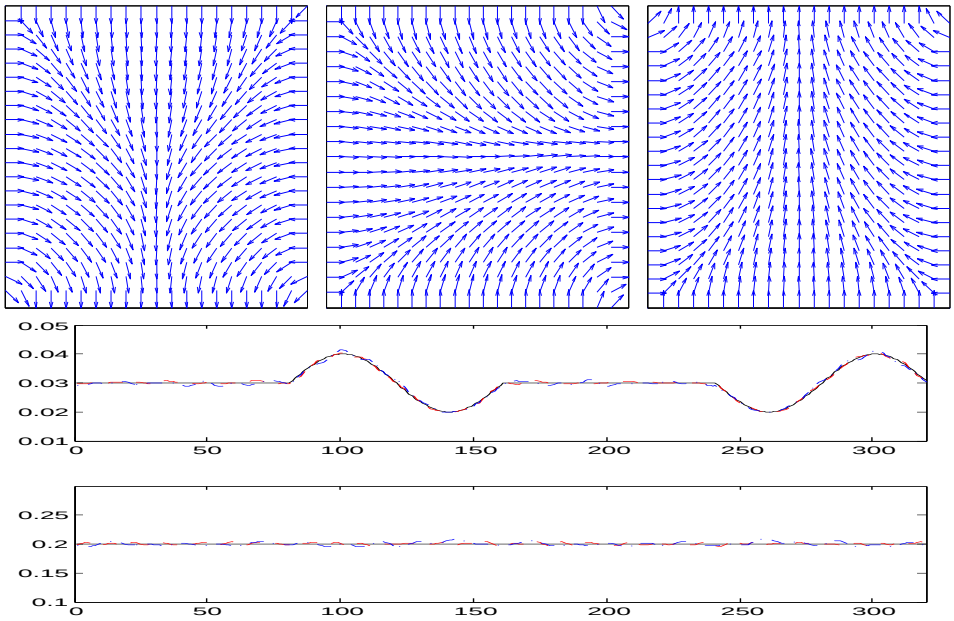

Figure 2: Top row: three vector fields; Bottom row: reconstructions of boundary values of D and σ on each part of the boundary.

The three vector fields constructed from the four sources are shown in Fig. 5 while the reconstructed coefficients are shown in Fig. 6. We do not observe significant differences between these reconstructions and those in the previous numerical experiments, as can be seen from the plots of the relative errors in the reconstructions. We also performed reconstructions with the linearization method, around the background coefficients. The results, not shown, are almost identical to the ones obtained with the nonlinear reconstructions, up to error caused by noise.

Experiment 5. We conclude this section by showing a numerical verification of the non-uniqueness result shown in Lemma 2.1. We do this by constructing two pairs of coefficients (D, σ) and $(\tilde{D}, \tilde{\sigma})$ that produces the same data $\mathbf{H} \equiv (H_1, H_2) = \tilde{\mathbf{H}} \equiv (\tilde{H}_1, \tilde{H}_2)$. To do that, we take a coefficient pair (D, σ) (including the boundary value) and construct (H_1, H_2) from this coefficient pair. We then follow the steps I-III in the proof of Lemma 2.1. We show in Fig. 7 two sets of coefficients (D, σ) (top left plots) and $(\tilde{D}, \tilde{\sigma})$ (top right plots) that lead to the same data sets $\mathbf{H} = (H_1, H_2)$ (bottom left plots). The two illuminations used in this case are the functions g_1 and g_2 defined in Experiment 1. We remark again that this non-uniqueness result does not contradict the uniqueness result in [8] because it is assumed there that the boundary values of the coefficients are known while here we assume that these boundary values are not known. This does not violate the uniqueness result in Theorem 2.2 either since we require the current data (9) in the Theorem 2.2. Indeed, we observe that the boundary data sets $\mathbf{J} = (J_1, J_2)$ and $\tilde{\mathbf{J}} = (\tilde{J}_1, \tilde{J}_2)$ are sufficiently different. We plot in the bottom right of Fig. 7 the relative differences between the currents, $\frac{J_1 - \tilde{J}_1}{J_1}$ (solid), on the bottom boundary of the domain and $\frac{J_2 - \tilde{J}_2}{J_2}$ (dashed) on the right boundary of the domain.

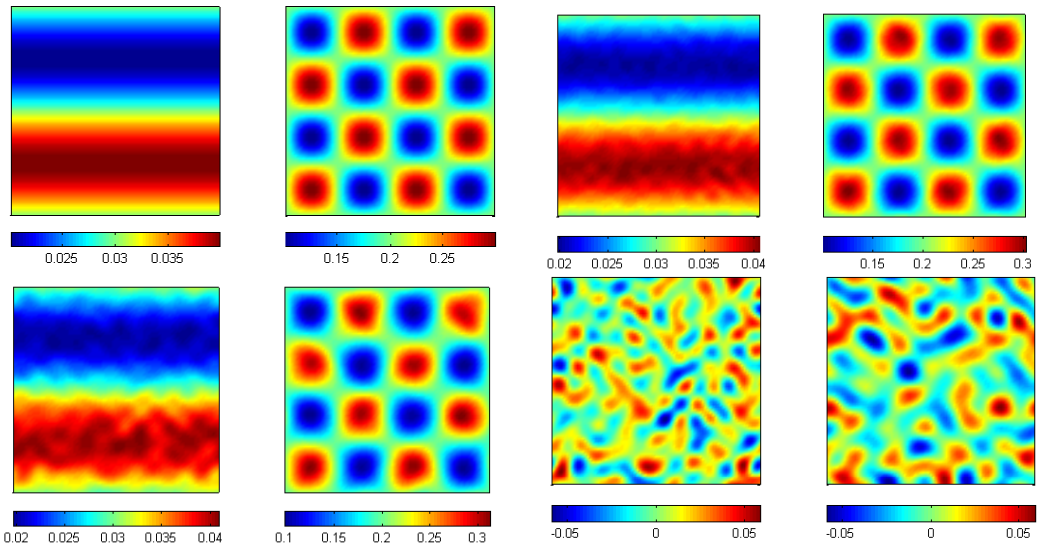

Figure 3: Reconstruction of smooth diffusion and absorption coefficients in Experiment 2. Show are real coefficients (top left), reconstructions with noiseless data (top right), reconstructions with noisy data (bottom left) and the relative difference between noisy reconstruction and the true coefficients (bottom right).

6 Conclusion and remarks

We present in this work a numerical reconstruction procedure for an inverse coefficient problem in quantitative photoacoustic tomography, aiming at reconstructing the absorption and diffusion coefficients in the diffusion equation. In order to recover the boundary values of the coefficients, we propose to combine diffuse optical tomography and photoacoustic tomography to obtain both boundary current data and interior absorbed energy distribution data, the later recovered from boundary acoustic measurements. We formulate the inverse problem as a nonlinear optimization problem, and then reduce the space of unknowns such that the boundary value of the diffusion coefficient is the only variable in the minimization problem.

Our numerical method combines a nonlinear minimization technique with an explicit reconstruction procedure that is proposed in [8, 9, 10]. We iteratively update the boundary value of the diffusion coefficient until the data generated by the model with such boundary value match the measured data. In each iteration, we solve the problem using the explicit vector field method to match the interior data. Compared to the explicit reconstruction in [8, 9, 10], our approach allows us to deal with the more realistic Robin boundary condition for the light diffusion model. Numerical simulations with synthetic data are presented to validate the method.

The method we propose in this paper can be generalized straightforwardly to the case when the Grüneisen coefficient is also treated as an unknown in the inverse problem. The non-dimensional Grüneisen coefficient Ξ measures the portion of the absorbed photon energy are converted into the initial pressure field. With this coefficient, the data H becomes $H = \Xi\sigma u$. The theory presented in [8] shows that one can not reconstruct all three coefficients

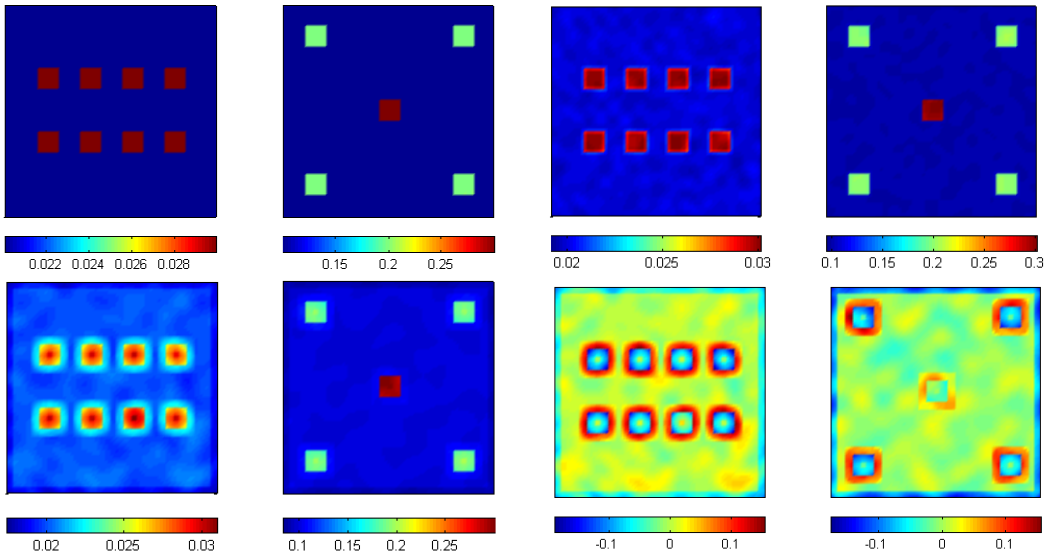

Figure 4: Same as Fig. 1 expect that the coefficients are now piecewise constant.

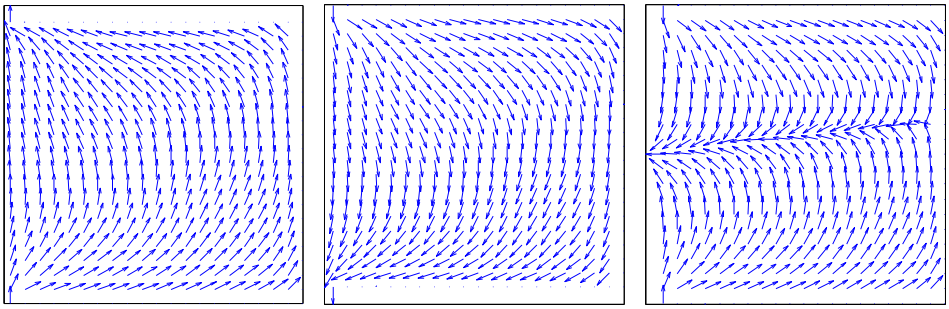

Figure 5: The three vector fields constructed from interior data collected for the illuminations in given in Experiment 4.

uniquely simultaneously. If one of the coefficient is known, then the other two can be reconstructed uniquely. Similar statements hold if we introduce Ξ here. When multi-spectral data are available, we can generalize our method as in [9] to reconstruct all three coefficients (D,σ, Ξ).

The idea of combining diffuse optical tomography with photoacoustic tomography seems to emerge recently in engineering community. In [36], the authors constructed an integrated diffuse optical tomography and photoacoustic tomography system and validated the approach with experimental phantom studies. This is the setting where the method we proposed in this work could be useful.

Acknowledgment

This work is partially supported by National Science Foundation through grant DMS-0914825 for KR, NSF grant DMS-1115698 and ONR grant N00014-11-1-0602 for HZ, and by the National Institute of Health/National Institute of Biomedical Imaging and Bioengi-

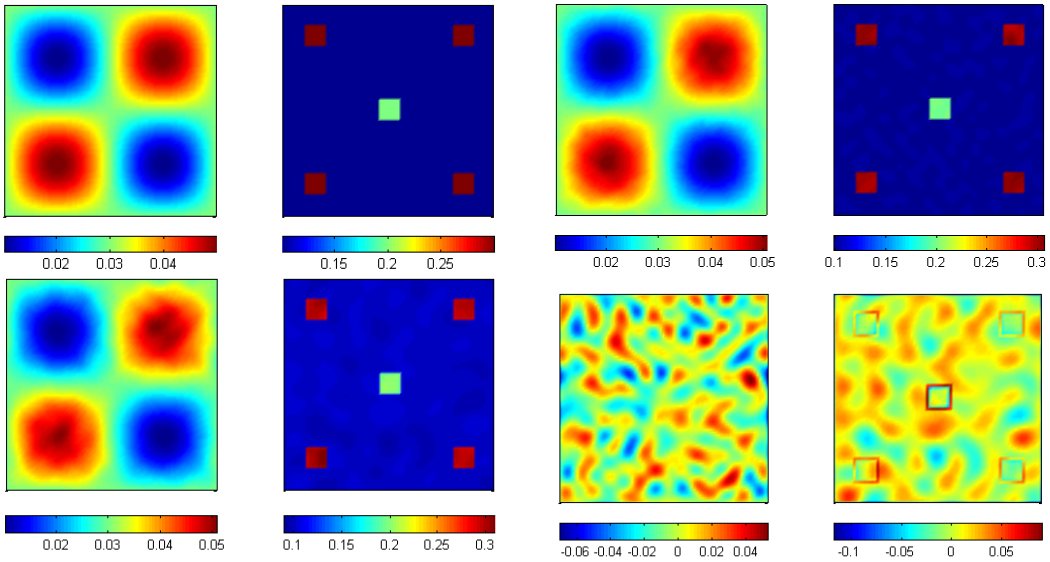

Figure 6: Reconstruction of diffusion and absorption coefficients in Experiment 4 with illuminations only on the left side of the boundary. Show are real coefficients (top left), reconstructions with noiseless data (top right), reconstructions with noisy data (bottom left) and the difference between noisy reconstruction and the true coefficients (bottom right).

neering 1R21EB013387-01A1 for HG.

References

[1] M. Agranovsky, P. Kuchment, and L. Kunyansky, *On reconstruction formulas and algorithms for the TAT and PAT tomography*, in Photoacoustic Imaging and Spectroscopy, L. V. Wang, ed., CRC Press, 2009, pp. 89–101.

[2] H. Ammari, *An Introduction to Mathematics of Emerging Biomedical Imaging*, Springer, 2008.

[3] H. Ammari, E. Bossy, V. Jugnon, and H. Kang, *Mathematical modelling in photo-acoustic imaging of small absorbers*, SIAM Rev., (2010).

[4] ——, *Quantitative photo-acoustic imaging of small absorbers*, SIAM J. Appl. Math., 71 (2011), pp. 676–693.

[5] S. R. Arridge, *Optical tomography in medical imaging*, Inverse Probl., 15 (1999), pp. R41–R93.

[6] G. Bal, *Hybrid inverse problems and internal information*, in Inside Out: Inverse Problems and Applications, G. Uhlmann, ed., Mathematical Sciences Research Institute Publications, Cambridge University Press, 2012.

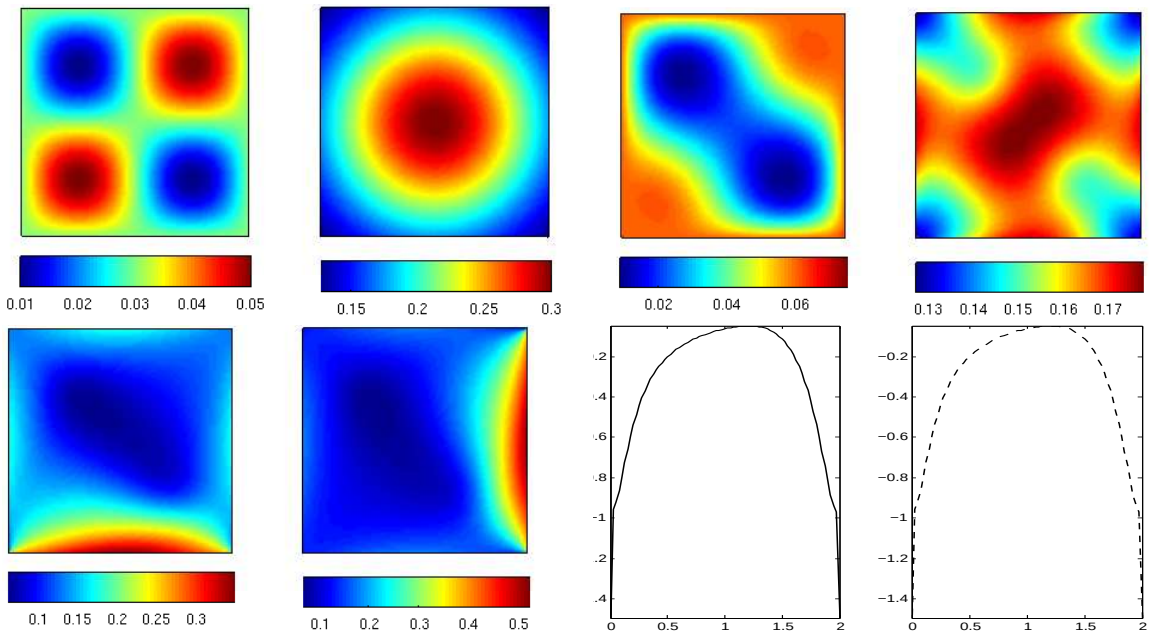

Figure 7: Two pairs of coefficients (D, σ) (top left) and $(\tilde{D}, \tilde{\sigma})$ (top right) that lead to the same interior data $\mathbf{H} = (H_1, H_2)$ (bottom left) but different boundary current data $\mathbf{J} = (J_1, J_2)$ and $\tilde{\mathbf{J}} = (\tilde{J}_1, \tilde{J}_2)$ (bottom right, shown are $\frac{J_1 - \tilde{J}_1}{J_1}$ (solid) and $\frac{J_2 - \tilde{J}_2}{J_2}$ (dashed)).

[7] G. Bal, A. Jollivet, and V. Jugnon, *Inverse transport theory of photoacoustics*, Inverse Problems, 26 (2010). 025011.

[8] G. Bal and K. Ren, *Multi-source quantitative PAT in diffusive regime*, Inverse Problems, 27 (2011). 075003.

[9] ——, *On multi-spectral quantitative photoacoustic tomography in diffusive regime*, Inverse Problems, 28 (2012).

[10] G. Bal and G. Uhlmann, *Inverse diffusion theory of photoacoustics*, Inverse Problems, 26 (2010). 085010.

[11] B. Banerjee, S. Bagchi, R. M. Vasu, and D. Roy, *Quatitative photoacoustic tomography from boundary pressure measurements: noniterative recovery of optical absorption coefficient from the reconstructed absorbed energy map*, J. Opt. Soc. Am. A, 25 (2008), pp. 2347–2356.

[12] R. H. Byrd, P. Lu, J. Nocedal, and C. Zhu, *A limited memory algorithm for bound constrained optimization*, SIAM J. Sci. Comput., 16 (1995), pp. 1190–1208.

[13] B. T. Cox, S. R. Arridge, and P. C. Beard, *Photoacoustic tomography with a limited-aperture planar sensor and a reverberant cavity*, Inverse Problems, 23 (2007), pp. S95–S112.

[14] ——, *Estimating chromophore distributions from multiwavelength photoacoustic images*, J. Opt. Soc. Am. A, 26 (2009), pp. 443–455.

[15] B. T. Cox, S. R. Arridge, K. P. Köstli, and P. C. Beard, *Two-dimensional quantitative photoacoustic image reconstruction of absorption distributions in scattering media by use of a simple iterative method*, Applied Optics, 45 (2006), pp. 1866–1875.

[16] B. T. Cox, J. G. Laufer, and P. C. Beard, *The challenges for quantitative photoacoustic imaging*, Proc. of SPIE, 7177 (2009). 717713.

[17] B. T. Cox, T. Tarvainen, and S. R. Arridge, *Multiple illumination quantitative photoacoustic tomography using transport and diffusion models*, Contemporary Mathematics, (2011).

[18] D. Finch, M. Haltmeier, and Rakesh, *Inversion of spherical means and the wave equation in even dimensions*, SIAM J. Appl. Math., 68 (2007), pp. 392–412.

[19] D. Finch and Rakesh, *The spherical mean operator with centers on a sphere*, Inverse Problems, 35 (2007), pp. S37–S50.

[20] H. Gao, S. Osher, and H. Zhao, *Quantitative photoacoustic tomography*, in Mathematical Modeling in Biomedical Imaging II: Optical, Ultrasound, and Opto-Acoustic Tomographies, H. Ammari, ed., Lecture Notes in Mathematics, Springer, 2012.

[21] H. Gao, H. Zhao, and S. Osher, *Bregman methods in quantitative photoacoustic tomography*. CAM Report 10-42, UCLA, 2010.

[22] D. Gilbarg and N. S. Trudinger, *Elliptic Partial Differential Equations of Second Order*, Springer-Verlag, Berlin, 2000.

[23] M. Haltmeier, O. Scherzer, P. Burgholzer, and G. Paltauf, *Thermoacoustic computed tomography with large planer receivers*, Inverse Problems, 20 (2004), pp. 1663–1673.

[24] M. Haltmeier, T. Schuster, and O. Scherzer, *Filtered backprojection for thermoacoustic computed tomography in spherical geometry*, Math. Methods Appl. Sci., 28 (2005), pp. 1919–1937.

[25] Y. Hristova, *Time reversal in thermoacoustic tomography - an error estimate*, Inverse Problems, 25 (2009). 055008.

[26] Y. Hristova, P. Kuchment, and L. Nguyen, *Reconstruction and time reversal in thermoacoustic tomography in acoustically homogeneous and inhomogeneous media*, Inverse Problems, 24 (2008). 055006.

[27] V. Isakov, *Inverse Problems for Partial Differential Equations*, Springer-Verlag, New York, second ed., 2002.

[28] C. T. Kelley, *Iterative Methods for Optimization*, Frontiers in Applied Mathematics, Society of Industrial and Applied Mathematics, Philadelphia, 1999.

[29] A. D. Klose and A. H. Hielscher, *Quasi-Newton methods in optical tomographic image reconstruction*, Inverse Probl., 19 (2003), pp. 387–409.

[30] P. Kuchment, *Mathematics of hybrid imaging. a brief review*, in The Mathematical Legacy of Leon Ehrenpreis, I. Sabadini and D. Struppa, eds., Springer-Verlag, 2012.

[31] P. Kuchment and L. Kunyansky, *Mathematics of thermoacoustic tomography*, Euro. J. Appl. Math., 19 (2008), pp. 191–224.

[32] ——, *Mathematics of thermoacoustic and photoacoustic tomography*, in Handbook of Mathematical Methods in Imaging, O. Scherzer, ed., Springer-Verlag, 2010, pp. 817–866.

[33] L. A. Kunyansky, *Explicit inversion formulae for the spherical mean Radon transform*, Inverse Problems, 23 (2007), pp. 373–383.

[34] J. Laufer, B. T. Cox, E. Zhang, and P. Beard, *Quantitative determination of chromophore concentrations from 2d photoacoustic images using a nonlinear model-based inversion scheme*, Applied Optics, 49 (2010), pp. 1219–1233.

[35] C. Li and L. Wang, *Photoacoustic tomography and sensing in biomedicine*, Phys. Med. Biol., 54 (2009), pp. R59–R97.

[36] X. Li, L. Xi, R. Jiang, L. Yao, and H. Jiang, *Integrated diffuse optical tomography and photoacoustic tomography: phantom validations*, Biomed. Opt. Express, 2 (2011), pp. 2348–2353.

[37] W. McLean, *Strongly Elliptic Systems and Boundary Integral Equations*, Cambridge University Press, Cambridge, 2000.

[38] A. Nachman, A. Tamasan, and A. Timonov, *Conductivity imaging with a single measurement of boundary and interior data*, Inverse Problems, 23 (2007), pp. 2551–2563.

[39] L. V. Nguyen, *A family of inversion formulas in thermoacoustic tomography*, Inverse Probl. Imaging, 3 (2009), pp. 649–675.

[40] J. Nocedal and S. J. Wright, *Numerical Optimization*, Springer-Verlag, New York, 1999.

[41] S. K. Patch and O. Scherzer, *Photo- and thermo- acoustic imaging*, Inverse Problems, 23 (2007), pp. S1–S10.

[42] J. Qian, P. Stefanov, G. Uhlmann, and H. Zhao, *An efficient Neumann-series based algorithm for thermoacoustic and photoacoustic tomography with variable sound speed*, SIAM J. Imag. Sci., (2011).

[43] K. Ren, G. Bal, and A. H. Hielscher, *Frequency domain optical tomography based on the equation of radiative transfer*, SIAM J. Sci. Comput., 28 (2006), pp. 1463–1489.

[44] J. Ripoll and V. Ntziachristos, *Quantitative point source photoacoustic inversion formulas for scattering and absorbing media*, Phys. Rev. E, 71 (2005). 031912.

[45] O. Scherzer, *Handbook of Mathematical Methods in Imaging*, Springer-Verlag, 2010.

[46] P. Stefanov and G. Uhlmann, *Thermoacoustic tomography with variable sound speed*, Inverse Problems, 25 (2009). 075011.

[47] D. Steinhauer, *A reconstruction procedure for thermoacoustic tomography in the case of limited boundary data*, Submitted, (2009).

[48] ——, *A uniqueness theorem for thermoacoustic tomography in the case of limited boundary data*, Submitted, (2009).

[49] L. V. Wang, *Ultrasound-mediated biophotonic imaging: a review of acousto-optical tomography and photo-acoustic tomography*, Disease Markers, 19 (2004), pp. 123–138.

[50] ——, *Tutorial on photoacoustic microscopy and computed tomography*, IEEE J. Sel. Topics Quantum Electron., 14 (2008), pp. 171–179.

[51] M. Xu and L. V. Wang, *Photoacoustic imaging in biomedicine*, Rev. Sci. Instr., 77 (2006). 041101.

[52] Z. Yuan, Q. Wang, and H. Jiang, *Reconstruction of optical absorption coefficient maps of heterogeneous media by photoacoustic tomography coupled with diffusion equation based regularized Newton method*, Optics Express, 15 (2007), pp. 18076–18081.

[53] R. J. Zemp, *Quantitative photoacoustic tomography with multiple optical sources*, Applied Optics, 49 (2010), pp. 3566–3572.